Inertial Sensors and Their Applications

Jussi Collin, Pavel Davidson, Martti Kirkko-Jaakkola, and Helena Leppäkoski

Abstract Due to the universal presence of motion, vibration, and shock, inertial motion sensors can be applied in various contexts. Development of the microelectromechanical (MEMS) technology opens up many new consumer and automotive applications for accelerometers and gyroscopes. The large variety of application creates different requirements to inertial sensors in terms of accuracy, size, power consumption and cost. It makes it difficult to choose sensors that are suited best for the particular application. Signal processing methods depend on the application and should reflect on the physical principles behind this application. This chapter describes the principles of operation of accelerometers and gyroscopes, different applications involving the inertial sensors. It also gives examples of signal processing algorithms for pedestrian navigation and motion classification.

1 Introduction to Inertial Sensors

Inertial sensors measure motion parameters with respect to the inertial space. They generally fall into two categories: (a) instruments sensing linear inertial displacement, also known as accelerometers, (b) rotational inertial rate sensors, also called angular rate sensors or gyroscopes.

J. Collin (✉) • P. Davidson • M. Kirkko-Jaakkola • H. Leppäkoski
Department of Pervasive Computing, Tampere University of Technology, Finland
e-mail: jussi.collin@tut.fi; pavel.davidson@tut.fi; martti.kirkko-jaakkola@tut.fi; helena.leppakoski@tut.fi

S.S. Bhattacharyya et al. (eds.), *Handbook of Signal Processing Systems*,
DOI 10.1007/978-1-4614-6859-2_3,

1.1 Accelerometers

An accelerometer is a device that measures translational acceleration resulting from the forces acting on it. This acceleration is associated with the phenomenon of weight experienced by a mass that resides in the frame of reference inside accelerometer and can be described by Newton's second law of motion: "A force **F** acting on a body of mass *m* causes the body to accelerate with respect to inertial space." A typical accelerometer consists of a small mass, also known as a proof or seismic mass, connected via a spring to the case of the instrument as shown in Fig. 1.

When the instrument experiences acceleration along its sensitive axis, the proof mass is displaced with respect to the case of instrument; this is the scenario in Fig. 1b. Under steady state conditions, the force acting on the mass will be balanced by the tension in the spring. The extension (or contraction) of the spring creates a force which is proportional to the displacement. When there is no drag force to resist the movement of the proof mass, its displacement is directly proportional to the acceleration. This way the applied acceleration can be measured by measuring the displacement of the proof mass.

There are many different designs for accelerometer but most of them operate in a manner similar to the simple spring and mass system described above. In many applications, including navigation, the three dimensional vector of acceleration is required. Normally, three single-axis accelerometers are used. In recent years, tri-axis instruments have become very popular in the segment of low-cost accelerometers. It is a common practice to mount the three accelerometers with their sensitive axes mutually orthogonal, although any non-coplanar configuration is acceptable as long as the angles between the sensitive axes are known.

Accelerometers are insensitive to the gravitational acceleration and unable to separate the total acceleration from that caused by the presence of a gravitational field. These sensors instead provide measurements of the difference between the true acceleration and the acceleration due to gravity. This quantity is the non-gravitational force per unit mass exerted on the instrument, and often called a

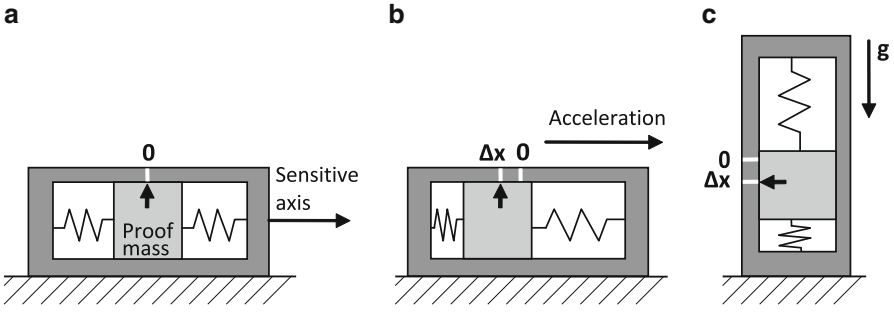

Fig. 1 A mass-and-spring accelerometer under different conditions: (**a**) at rest or in uniform motion, (**b**) accelerating, and (**c**) at rest

specific force. For example, if we consider an accelerometer in free fall, the case and the proof mass will fall together. Therefore, there will be no displacement of the proof mass with respect to the case and the output of the instrument will remain at zero. In other words, the acceleration $\mathbf{a}$ of the instrument with respect to an inertially fixed set of axes equals the gravitational acceleration $\mathbf{g}$ and the specific force is zero. If the accelerometer is held stationary, i.e. $\mathbf{a} = \mathbf{0}$, it will measure the force which is counteracting to stop it from falling, $\mathbf{f} = -m\mathbf{g}$, as visualized in Fig. 1c. This specific force is required to offset the effect of gravitational attraction. Therefore, the measurements provided by the accelerometer must be combined with knowledge of the gravitational field in order to determine the acceleration of the sensor unit with respect to the inertial space.

The various accelerometer technologies include [29]: mechanical, surface acoustic waves, piezoelectric, fiber optic, vibrating beam and solid-state microelectromechanical (MEMS) accelerometers. Historically, mechanical accelerometers were the first type of accelerometers in mass production. All mechanical accelerometers are mass–spring type sensors. They can be implemented in open loop when a displacement of a proof mass with respect to its "null" position is proportional to the specific force applied along its input axis. They can be also implemented as closed loop or force feedback pendulous accelerometer in which the spring is replaced by an electromagnetic device that produces force on the proof mass to maintain it at its "null" position. The most precise mechanical force-feedback pendulous accelerometers are capable of measuring specific force with resolutions of micro-g or better. This class of mechanical accelerometers is used in very accurate (navigation grade) inertial navigation systems (INS).

Most of accelerometers nowadays are manufactured using MEMS technology that was developed for the military and aerospace markets in the 1970s. In 2010, the production volume of MEMS accelerometers was about 1.2 billion units, dominated by consumer electronics and automotive applications. MEMS accelerometers can be fabricated in many different ways. The basic process modules include bulk micromachining, surface micromachining, wafer bonding, and deep reactive-ion etching (DRIE). In most cases, the fabrication involves a combination of two modules or more. The majority of the commercial accelerometers are surface micromachined. One advantage of surface micromachining is its potential of Complementary Metal-Oxide-Semiconductor (CMOS) integration. However, due to some technical challenges, two-chip solutions are still dominant in commercial products. Bulk micromachining is often combined with wafer bonding (glass–silicon or silicon–silicon) to produce high-performance accelerometers. A recent development in which single crystal silicon (SCS) sensing elements are created in CMOS substrate by using DRIE shows some promising results. In terms of materials, almost all MEMS accelerometers are made of silicon including silicon on insulator (SOI). More about MEMS accelerometers can be found in [8, Chapter 2.05].

1.2 Gyroscopes

Gyroscope (or gyro for short) is a device for measuring or maintaining angular orientation. It can measure turn rates caused by changes in attitude with respect to inertial space. Historically the first sensors of this kind were mechanical gyros. They exploit the inertial properties of a wheel spinning at high speed, which tends to keep the direction of its spin axis due to the principles of conservation of angular momentum. Although the axle orientation does not remain fixed, it changes in response to an external torque much less and in a different direction than it would without the large angular momentum associated with the disc's high rate of spin and moment of inertia. Since external torque is minimized by mounting the device in gimbals, its orientation remains nearly fixed, regardless of any motion of the platform on which it is mounted. There are several designs for mechanical gyros including: dynamically tuned gyroscope (DTG), flex gyro, and dual-axis rate transducer (DART) which is suitable only for low accuracy applications [29].

Following the development of spinning mass gyros, other kinds of angular rate sensors, such as optical and vibrating gyros, were developed [3]. These sensors are based on different physical principles than the conservation of angular momentum. Optical gyros are based on the Sagnac effect which causes a phase shift between two waves counter-propagating in a ring interferometer that is rotating; the shift is proportional to the rate of rotation. Vibrating gyros are based on Coriolis effect that induces a coupling between two resonant modes of a mechanical resonator. Optical gyros can be effectively implemented using different integrated optics technologies that generally fall into two categories: (a) ring laser gyroscopes (RLG) and (b) fiber optics gyroscopes (FOG). RLGs can be made very accurate to meet the requirements for navigation grade, but on the other hand, they are expensive, their size increases with performance, and they are high-voltage devices. FOGs are less accurate compared to RLGs, but they meet the requirements of medium accuracy (tactical grade), medium cost gyroscopes.

Vibrating gyros are usually manufactured using MEMS technology [8, Chap. 2.06]. From the accuracy point of view, MEMS gyros are of low to medium accuracy with their performance approaching FOG. They have low manufacturing costs, small physical size, and low power consumption; moreover, they can survive severe shocks and temperature changes. Therefore, MEMS technology is ideally suited for mass production.

1.3 Areas of Application

Due to the universal presence of motion, vibration, and shocks, inertial sensors can be applied almost everywhere, from aircraft and space navigation to underground drilling, from hard disk fall protection to airbags in vehicles, and from video games to performance improvement of athletes. The large variety of applications

creates different requirements to inertial sensors in terms of accuracy, size, power consumption, and cost. For example, the principal driving force for high-accuracy inertial sensors development has been inertial navigation for aircraft and submarines, precise aiming of telescopes, imaging systems, and antennas. For some applications, improved accuracy is not necessarily the most important issue, but meeting performance at reduced cost and size is. The major requirements to inertial sensors in automotive industry are low cost, high reliability, and possibility of mass production. In the following sections some examples of applications are given.

1.3.1 Navigation

INSs normally consist of three gyros and three accelerometers. The data from inertial sensors are processed to calculate the position, velocity, and attitude of the vehicle. High performance INSs require accurate sensors. Such systems are expensive, weigh several kilos, and have significant power consumption. However, not in every navigation application has a high-performance INS to be used. For example, land vehicle navigation systems can significantly reduce INS error growth by applying non-holonomic constraints[1] and using odometer measurements. Therefore, in many land vehicle applications a lower cost tactical grade INS can be used instead of a more expensive navigation grade INS. Pedestrian navigation systems take advantage of biomechanics of walking. Recognizing that people move one step at a time, the pedestrian mechanization restricts error growth by propagating position estimates in a stride-wise fashion, rather than on a fixed time interval. Inertial sensors are used to detect the occurrence of steps, and provide a means of estimating the distance and direction in which the step was taken. For step detection, accelerometers don't have to be of high accuracy. Pedestrian navigation is addressed more profoundly in Sect. 3.

1.3.2 Automotive

In modern cars, MEMS accelerometers are used in airbag deployment systems to detect a rapid negative acceleration of the vehicle, determine if a collision occurred, and estimate the severity of the collision. Another common automotive use of MEMS gyros and accelerometers is in electronic stability control systems. It compares the driver's intended direction which can be determined through the measured steering wheel angle to the vehicle's actual direction determined through measured lateral acceleration, vehicle yaw rotation, and individual wheel speeds. Other automotive applications include monitoring of noise, vibration, harshness, and conditions that cause discomfort for drivers and passengers and may also be indicators of mechanical faults.

[1] In short, non-holonomic constraints allow to neglect the lateral and vertical speeds of the vehicle.

1.3.3 Industrial

In industrial applications accelerometers are widely used to monitor machinery vibrations. Analysis of accelerometer based vibration data allows the user to detect conditions such as wear and tear of bearings, shaft misalignment, rotor imbalance, gear failure, or bearing fault in rotating equipment such as turbines, pumps, fans, rollers, compressors, and cooling towers. The early diagnosis of these faults can prevent costly repairs, reduce downtime, and improve safety of plants in such industries as automotive manufacturing, power generation, pulp and paper, sugar mills, food and beverage production, water and wastewater, hydropower, petrochemistry, and steel production.

1.3.4 Consumer Products

The availability of small size tri-axis accelerometers and gyroscopes with prices less than $2 has opened up new markets for inertial sensors in video game controllers, mobile phones, cameras, and other personal electronic devices. The applications of inertial sensors in consumer devices can be divided into the following categories: (a) orientation sensing, (b) gesture recognition, (c) motion input, (d) image stabilization, (e) fall detection, and (f) sport and healthy lifestyle applications.

The most common application of orientation sensing by accelerometers is converting the display to a horizontal or vertical format based on the way the device is being held. For example, the Apple iPhone 4 contains an STMicroelectronics LIS331DH tri-axis accelerometer in and an L3G44200D tri-axis gyroscope that allow the device to know its orientation and when it is tilted on its side. Third-party developers for iPhone have created thousands of motion-sensitive games and other fanciful applications with orientation sensing features. With the use of the Global Positioning System (GPS) and a magnetic compass, location-based services are enabled, making it possible to identify special sales or lunch menus by just pointing a cell phone at a building.

Computer or video games can exploit gesture recognition techniques and make it possible to play the games or do virtual activities such as swinging a tennis racket or drive a vehicle by moving a hand-held controller. Nintendo's Wii video game console uses a controller called a Wii Remote that contains a tri-axis accelerometer and was designed primarily for motion input. The Sony PlayStation 3 uses the DualShock 3 remote with embedded tri-axis accelerometer that can be used to make steering more realistic in racing games, such as Motorstorm and Burnout Paradise.

Commonly used example of motion input application is darkening the display when not needed by detecting the motionless state. Some smartphones use accelerometers for user interface control, for example, make selections by scrolling down a list by tilting. The accelerometer-enabled wireless mouse makes it possible to move an object in space and have a corresponding object or cursor follow in a computer-generated visual model.

Cameras use inertial sensors for image stabilization to reduced blurring associated with the motion of a camera during exposure. It compensates for angular yaw and pitch movement of the camera. There are two ways for images stabilization in cameras: (1) make adjustments to the image sensor or the lenses to ensure that the image remains as motionless as possible, (2) digital image stabilization in which the physical image is allowed to track the scene on the sensor by software to produce a stable image. The digital technique requires the pixel count to be increased to allow the image to move on the sensor while keeping reference points within the boundaries of the capture chip. Different companies have different names for their image stabilization technology: Image Stabilizer (Canon), Vibration Reduction (Nikon), Optical SteadyShot (Sony Cyber-Shot), Super SteadyShot (Sony), MEGA Optical Image Stabilizer (Panasonic and Leica), Optical Stabilizer (Sigma), Vibration Compensation (Tamron) and Shake Reduction (Pentax).

Fall detection is an important safety feature to protect hard disk drives in laptops and some other portable, "always on" devices like MP3 players. Many of these devices feature an accelerometer which is used to detect drops. If a drop is detected, the heads of the hard disk are parked to avoid data loss and possible head or disk damage caused by the shock.

1.3.5 Sport

Pedometer is an example of application that can encourage a healthy lifestyle. A pedometer in its simplest form is a step counter and can be implemented using low-cost accelerometers. Other examples of inertial sensors in sport include motion analysis such as golf swing, figure skating jumps, and trajectory analysis in ski jumping and javelin. Xsens MVN Motion Capture [24,33] is an interesting example of how inertial sensors can be used to record human movement. The motion capture suit includes 17 inertial trackers strapped to the different parts of the body. The data can be used in medical and sports applications to analyze human movement and gait. It can be also used to animate digital characters in movies, games, and virtual environments.

2 Performance of Inertial Sensors

Selection of the most suitable inertial sensors for a particular application is a difficult task. Among the parameters that have to be considered are resolution, dynamic range, accuracy, cost, power consumption, reliability, weight, volume, thermal stability, and immunity to external disturbances. Usually when sensors are examined for compliance, accuracy is the first parameter to start with.

All accelerometers and gyros are subject to errors which limit their accuracy in the measurement of the applied acceleration or angular rate. The measurement error is defined as the difference between the measured and the true value of the

physical quantity. Generally, inertial sensor errors fall into two broad categories: (a) systematic errors and (b) random errors. When measurement errors are analyzed, the same methodology can be applied to gyros and accelerometers.

Systematic errors are measurable and sensor type specific. They are caused by inaccuracy of system parameters and parasitic effects, streaming from the sensor design, its fabrication processes, and the readout electronics. In the context of MEMS sensors, systematic errors apply to whole batches of sensors of a certain type produced by the same process.

Random errors are caused by interference, noise, instability etc. They can be divided into two groups: (a) wideband or uncorrelated noise and (b) colored or correlated noise. Examples of uncorrelated noise are thermal noise [19] and quantization errors in the analog-to-digital conversion of the output signal. These errors can be modeled as additive Gaussian white noise process. The effect of zero-mean white noise can be mitigated by averaging the signal over longer periods of time; since the output rate of inertial sensors is typically very high (e.g., $1,000\,\text{Hz}$), the signals are usually down-sampled to a slower update rate by averaging.

Correlated noise is a more complicated and much more diverse phenomenon. Some examples of correlated noise are random walk, Markov processes, and flicker noise. Flicker or $1/f$ noise is a nonstationary, long-memory process (i.e., its autocorrelation decays slower than exponentially) [14]. The name stems from the fact that the power spectral density of $1/f$ noise is inversely proportional to the frequency; this implies that a major part of the power of the noise is located at low frequencies. In the context of inertial sensors, this noise process is also referred to as bias instability [9], but in this chapter, we will use the term $1/f$ noise to refer to this process and reserve the term "bias instability" for characterizing sensor quality (see Sect. 2.1).

$1/f$ noise has been observed in a wide range of different contexts, such as semiconductors, time standards, and highway traffic; even the ancient records of river Nile's flood levels have a $1/f$ power spectral density [30]. However, the origin of the phenomenon is not known, but it seems that there is no common physical mechanism to cause it in all these contexts [14]. Therefore, in order to model inertial sensor errors accurately, the contribution of $1/f$ noise must be handled carefully. A common tool for characterizing the contributions of the different noise types is the Allan variance which is described in Sect. 2.1.2. Other characterization methods do exist [17], but using Allan variance is recommended in [10].

2.1 Effect of Different Sources of Error

When analyzing the measurement errors of inertial sensors, it is a common practice to split the measurement error into several components that are mutually independent and specific to different modes of operation. For instance, even if the applied input signal is absent, the sensor output is not zero; this error source is called an offset or *bias*. Therefore, the bias is defined as the average of sensor output over

a specified time interval that has no correlation with the input signal. Accelerometer bias is measured in m/s^2 or fractions of g whereas gyro bias is measured in $^\circ$/h or $^\circ$/s. In many cases the bias is not exactly constant but changes slowly in time. This phenomenon is also called *bias instability* and can be quantified as the peak-to-peak amplitude of the long-term bias drift.

The next important error component is the *scale factor error* which is defined as the error in the ratio relating the change in the output signal to a change in the applied input signal. Scale factor error is commonly expressed as a ratio of output error to input rate in parts per million (ppm), or, especially in the lower performance class, as a percentage figure.

Cross-axis sensitivity errors result from the sensor's sensitivity to signals applied about axes that are perpendicular to the sensitive axis. Such errors can be due to physical misalignments of the sensors' sensitive axes or, particularly in the case of MEMS sensors, electromagnetic interference between the channels. The cross-axis sensitivity is also expressed in ppm or a percentage of the applied acceleration or angular rate. *Linearity* (non-linearity) error is defined as the closeness of the calibration curve to a specified straight line. The *acceleration-dependent bias* (*g*-dependent bias) is an error which occurs in gyroscopes only; it is proportional to the translational acceleration of the sensor.

All the error sources mentioned above consist of both systematic and random errors.

2.1.1 Calibration of Inertial Sensors

Calibration refers to correcting a measuring device by adjusting it to match reference values. Calibration of inertial sensors can significantly improve their performance. Long-term errors, i.e., those which remain constant for at least 3–5 years, can be corrected for in the factory. The factory calibration usually includes temperature compensation to guarantee good performance over the entire operational temperature range. This calibration eliminates a significant part of the measurement errors. The residual errors are much smaller than the initial errors and can be explained by the fact that the bias and scale factor errors can slightly change when the system is turned on next time—the so-called *day-to-day* error. Furthermore, the temperature compensation does not eliminate all errors caused by temperature variations.

Despite the fact that the residual errors are much smaller than the errors before the factory calibration, the sensors' performance can be improved even further if these residual errors are calibrated out. The approach for calibration of these errors depends on the application, the measurement scenario, and the type of error. From the system's perspective, one can approach the errors and their correction based on the sensor transfer characteristic (static and dynamic). With the emergence of digital signal processing and its use with sensors, this approach is becoming the standard. Keeping in mind that all sources of measurement error cumulatively affect the accuracy and resolution of a sensing system in a negative manner, the systems

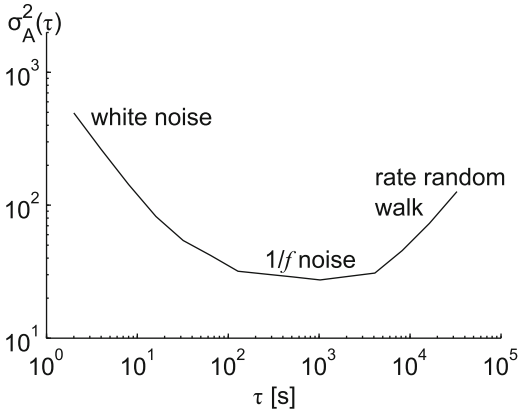

Fig. 2 An example Allan variance plot

obey the principle of "a chain only being as strong as its weakest link". Errors such as interference, noise, and instability could be eliminated through chopping or dynamic amplification and division applied to individual sensors.

2.1.2 Allan Variance

Named after Dr. David W. Allan, the Allan variance [1] is a quantity to characterize the stability of oscillator systems. Although originally developed for frequency standards, the Allan variance is widely used to characterize the performance of inertial sensors; it reveals the contributions of uncorrelated and random walk type error processes on the measurement noise. The Allan variance σ_A^2 is a function of the averaging time τ, computed as

$$\sigma_A^2(\tau) = \frac{1}{2(N-1)} \sum_{i=1}^{N-1} \left(\bar{y}_\tau(i+1) - \bar{y}_\tau(i)\right)^2 \tag{1}$$

where the data y have been partitioned into N disjoint bins of length τ, and $\bar{y}_\tau(i)$ is the average value of the ith such bin. The square root of Allan variance is known as the Allan deviation, which is in accordance with common statistical terminology.

Usually, the Allan variance function is visualized as a log–log graph; an example is shown in Fig. 2. Generally, the Allan variance curve is U-shaped. At short averaging times, uncorrelated noise dominates the output. The variance of independent and identically distributed data is inversely proportional to the averaging time, which causes a negative slope to the Allan variance at short averaging times. As the averaging time increases, after some point, $1/f$ noise starts to dominate over uncorrelated noise and the curve levels off—the Allan variance of $1/f$ noise is constant [30]. Eventually, the curve starts to increase due to rate random walk.

Based on the Allan variance plot, it is possible to quantify certain characteristics of the sensor noise. The variance of white noise can be estimated as the Allan

variance where τ equals the sampling period. Furthermore, the value of Allan variance at the flat bias instability region is directly related to the power of $1/f$ noise [30]. Finally, the rate random walk slope shows the drift characteristics of the additive bias. There are also other phenomena that can be identified using Allan variance [10], but the effects discussed above are usually the most significant.

2.1.3 Modeling the Measurement Errors

A key to estimating and compensating for inertial sensor measurement errors is an accurate model of the evolution of the different error components with time. Some of the most commonly encountered models of sensor error time series $x(t)$ are

- *random constant*
$$x(t) = x(t-1); \tag{2}$$
- *first-order Gauss–Markov* (GM) models of the form [5]
$$x(t) = \mathrm{e}^{-\Delta t/\gamma} x(t-1) + \eta(t) \tag{3}$$
where Δt is the time interval between steps, γ is the *correlation time* of the process, and $\eta(i)$ are independent zero-mean Gaussian random variables; and
- *random walk*
$$x(t) = x(t-1) + \eta(t) \tag{4}$$
where the random increments $\eta(i)$ are independent and zero-mean (but not necessarily Gaussian).

These three models are closely related. It can be seen that when the correlation time γ tends to infinity, GM approaches the random walk process. On the other hand, with $\gamma \to 0$, GM tends to white noise. Random walk and GM processes are examples of *autoregressive* (AR) models which are more generally expressed as

$$x(t) = \sum_{i=0}^{t-1} a(i)x(i) + \eta(t) \tag{5}$$

where $a(i)$ are known coefficients and $\eta(i)$ are independent zero-mean random variables. Sometimes the noise process η is called the driving noise. Figure 3 shows an example realization of white noise along with the random walk and GM processes ($\gamma = 300$ samples) generated using the same noise. It can be seen that the correlated processes have significantly higher values than their driving noise.

Usually, scale factor errors are quite stable over time and can be modeled as random constants.[2] In contrast, the bias of an inertial sensor can vary significantly

[2]Scale factors are not exactly constant: for instance, the scale factors of MEMS sensors depend strongly on the temperature.

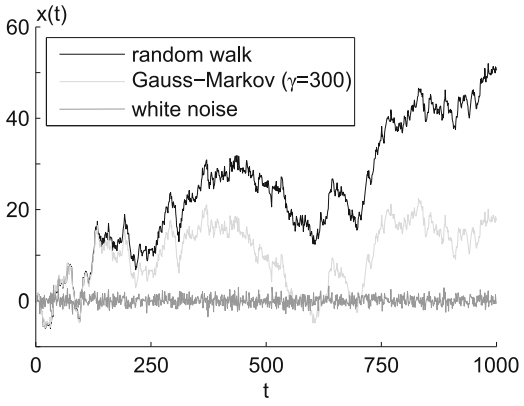

Fig. 3 Example realizations of white noise, random walk, and a first-order Gauss–Markov process

during operation, particularly in the case of MEMS sensors. Therefore, sensor biases are often modeled as GM or random walk processes. It should be noted that they are *Markovian* processes, i.e., the value of the process at time t only depends on the state of the process at $t-1$, not on other past or future states.[3] Thus, they are suboptimal for modeling the $1/f$ bias instability process which is known to have a long memory.

It is possible to model $1/f$ processes as AR processes [15]. However, optimal modeling of a long-memory process requires an infinite number of states to be memorized [26]; for this reason, many authors have fitted finite-order AR models on sequences of data in order to predict the future behavior of, e.g., a gyroscope's bias.

2.2 Sensor Quality Grade

Inertial sensors are used for various purposes and not all use cases demand similar performance. For instance, the requirements for the gyroscope of an automotive stability control system are significantly different from the requirements for full six-degrees-of-freedom inertial navigation. Traditionally, inertial sensors have been categorized into several grades based on their performance.

Navigation grade sensors are targeted for long-term autonomous navigation whereas *tactical grade* systems are manufactured for shorter intervals of navigation, usually a few minutes. Typically, the required performance for a navigation-grade system can be that the position error must not increase by more than one nautical mile (1.85 km) after one hour of autonomous inertial navigation. For example, navigation grade sensors can be needed for navigation systems in aircraft while a tactical grade unit can be sufficient for a missile.

[3] There exist higher-order Gauss–Markov process where the difference equation (3) contains older values of the process.

Table 1 Example specifications for IMUs of different quality grades

Parameter		Unit	Navigation	Tactical	Consumer
Accelerometer	Pre-calibration bias	m*g*	0.050	1	10
	Scale factor error	%	0.002	0.03	1
	Misalignment	mrad	0.05	0.5	–
	Cross-axis sensitivity	%	–	–	1
Gyroscope	Pre-calibration bias	°/h	0.005	1	1 000
	Bias instability	°/h	0.0035	1	25
	Angular random walk	$°/\sqrt{h}$	0.005	0.125	2
	Scale factor error	%	0.001	0.015	1
	Misalignment	mrad	0.01	0.5	–
	Cross-axis sensitivity	%	–	–	1
IMU	Weight	kg	5	1	0.01[a]
	Volume	cm^3	5000	500	30[a]
	Power consumption	W	10	5	0.3

[a] The physical dimensions of a MEMS IMU depend on the readout electronics etc

Consumer or *automotive* grade sensors are not capable of autonomous navigation, but can be used for positioning temporarily, e.g., when satellite based positioning is not available, such as when driving through an underpass. Consumer grade sensors are primarily installed for other purposes than navigation; examples of applications are given in Sect. 1.3.

Table 1 shows example specifications of different grades of inertial measurement units (IMUs); the values are examples only and should not be used as a definition of the different quality levels. Anyway, it is clear that the gap between consumer and navigation grades is large—the differences are in the order of many decades. Misalignment errors have not been specified for consumer-grade units because it is difficult, if not impossible, to separate their misalignment errors from other cross-coupling effects such as inter-channel electromagnetic interference; hence, the total cross-axis sensitivity is given for these IMUs instead. It should also be noted that the size of a MEMS IMU depends on many factors, such as the readout electronics; the sensor chip itself can be significantly smaller than the example values given in Table 1. Anyway, it is clear that MEMS instruments are smaller than, e.g., optical gyroscopes by orders of magnitude.

When considering the performance parameters and requirements of sensors, it is important to distinguish between errors before calibration and residual errors [25]. For instance, the large bias of a consumer gyroscope can be mostly compensated for by frequent calibration (e.g., whenever the IMU is stationary), but the bias instability ultimately determines the attainable performance. On the other hand, with high-quality IMUs it may be possible to calibrate out misalignment errors to an accuracy better than the physically achievable sensor alignment precision.

3 Pedestrian Dead Reckoning

In inertial navigation the data from three accelerometers and three gyroscopes are used to update position estimates. Position estimation with INS involves double-integration of acceleration measurements and transformation of measured accelerations from the coordinate frame of sensor unit to a local level coordinate frame, e.g. east-north-up (ENU) frame. This coordinate transformation is obtained using information on the attitude of the sensor unit; the attitude estimation involves integration of gyroscope measurements. The tasks of maintaining attitude estimate and double-integration of accelerations are called INS mechanization.

In the double-integration of accelerations, even a small error in acceleration measurement yields a large position error drift in the output. Because the accelerometers measure the specific force instead of the true acceleration of the sensor unit, the gravitational acceleration is added to the vertical acceleration component; this is easy when the accelerations are expressed in locally level frame. However, because the gravity compensation of accelerations require the coordinate transformation, any error in gyroscope output causes errors in the transformed accelerations, which in turn introduces increasing errors to the computed accelerations through the errors in the gravity compensation. As the gyro outputs are integrated to form the coordinate transformation and the transformed accelerations are double-integrated for position estimate, the gyro errors produce a position error which increases with time cubed. Therefore the gyro performance is very critical in INS implementations.

As the requirements for sensor accuracies are very strict for INS mechanization, requiring very high-quality and expensive sensor units, the developers of mass-market applications are looking for solutions where multiple integrations of sensor errors can be avoided. Pedestrian Dead Reckoning (PDR) is one way to reduce the effects of accelerated accumulation of sensor errors. The term *dead reckoning* (DR) refers to the method where a new position estimate is computed by adding measured or estimated displacements to the coordinates of a known starting point. In PDR, instead of double-integration of the accelerations, the speed of the walk is estimated from the periodical acceleration waveform produced by pedestrian movements. The speed can be estimated either from the main frequency of the periodic signal or by detecting individual steps and estimating their lengths and durations from the acceleration waveform. This information along with estimated heading is used to propagate the estimate of user position. It can be shown that PDR mechanization is superior to the traditional INS mechanization for a person on foot [22]. The main drawback of PDR is the limitation to one motion mode; the mechanization works only when walking while INS works without any assumptions about the user motion.

3.1 Step Detection with Accelerometers

With *step* we mean the displacement of one foot during walking movement, i.e. the distance between two consecutive foot prints. The occurrence of a step can be easily detected from the signal pattern of the vertical acceleration component [20, 21]. However, this approach is sensitive to orientation errors of the sensor unit, as it is assumed that one axis is aligned with vertical or that the transformation to the vertical is known. Other possibility it to compute the magnitude of the measured acceleration vector, i.e. the norm of acceleration [13].

The signal pattern varies according to where the user attaches the sensor unit [18]. Typical choices to wear the sensor unit are on the belt, e.g. on the side of the user or on lower back, or onto upper parts of the torso, e.g. attach it to the shoulder strap of a backpack or wear it in a chest pocket. Another option is to mount the sensor unit to the shoe of the pedestrian. With a shoe mounted sensor unit the estimation of the distance traveled can be based on the analysis of the acceleration waveform [27] or, if sensor unit includes high quality gyros, also traditional INS mechanization with zero-velocity updates can be used [7]. In this presentation, only PDR systems using torso mounted sensors are considered in detail.

Step detection is often based on the detection of signal peaks [18] or crossings of the signal with its average [13] or some other reference level [21]. For example, step detection from acceleration norm consists of the following steps:

1. Low pass filtering and resampling the signal; sampling frequency in the range 20–25 Hz is high enough.
2. Computation of the norm of current acceleration sample, i.e.,

$$a_n(t) = \sqrt{a_x(t) + a_y(t) + a_z(t)} \tag{6}$$

   where $a_n(t)$ is the acceleration norm and $a_x(t)$, $a_y(t)$, and $a_z(t)$ are the filtered components of the measured acceleration.
3. Instances of step starts $t_s(k)$ are detected by observing the g-crossings of the acceleration norm that are followed by a rise rate and a peak height that exceed the preset limits, and requiring that the time between the current and previous g-crossings is long enough.
4. The step end $t_e(k)$ is considered to be found when the next step starts or when a predefined time, considered as the maximum duration of one step, has passed after the start of the current step.

An example with acceleration norm and the detected step starts is shown in Fig. 4. The data for the figure were recorded using a sensor unit that was attached to the belt and positioned to the back of the test walker.

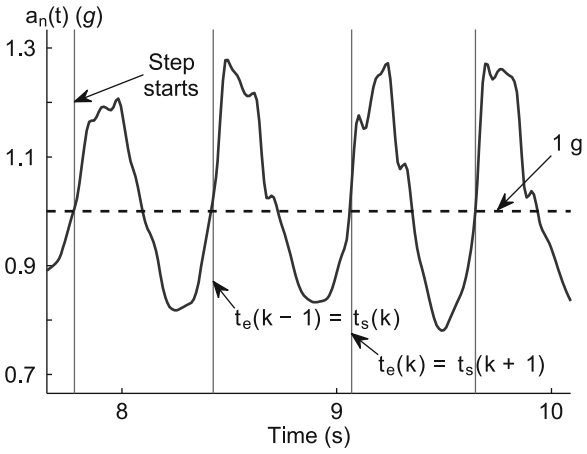

Fig. 4 Detection of steps from acceleration norm

3.2 Step Length Estimation

There are two main categories for methods to estimate step length. The first category includes models that are based on the biomechanical principles whereas the models in the second category are based on empirical relationships between acceleration signal pattern and step length. With biomechanical models, certain user-related parameters, such as leg length, are needed in addition to the empirically determined scaling parameters [11]. In empirical models, the acceleration norm $a_n(t)$ or the vertical acceleration component $a_v(t)$ are typically used for step length estimation. The signal patterns that have good correlation with step length include the following:

- Main frequency of the periodical signal [18, 20] which can be obtained from FFT or by computing the inverse of step duration determined by step detection algorithm

$$p_1(k) = 1/(t_e(k) - t_s(k)) \tag{7}$$

- Variance of the acceleration signal over a time window comparable to some step durations [18], e.g. variance over one step

$$p_2(k) = \mathrm{var}(a_n(t)), \qquad t_s(k) \le t < t_e(k) \tag{8}$$

or

$$p_3(k) = \mathrm{var}(a_v(t)), \qquad t_s(k) \le t < t_e(k) \tag{9}$$

- Integral of the absolute value acceleration norm where local gravity has been subtracted, integrated over the duration of the step [13]

$$p_4(k) = \int_{t_s(k)}^{t_e(k)} |a_n(t) - g| \, dt \tag{10}$$

- Difference between the maximum and minimum acceleration of a detected step [11]

$$p_5(k) = \max a_n(t) - \min a_n(t), \qquad t_s(k) \le t < t_e(k) \tag{11}$$

or

$$p_6(k) = \max a_v(t) - \min a_v(t), \qquad t_s(k) \le t < t_e(k). \tag{12}$$

Also the use of combinations of these signal patterns has been proposed [11, 18], as well as slightly different patterns from these [21]. The empirical step length model often includes at least one empirically determined parameter. In many cases a non-linear function, such as raising to a power or extraction of root, has to be applied to the signal pattern. In the following example, the performance of step length estimation with different functions applied on different signal patterns is demonstrated with real pedestrian data.

Example: Comparison of Functions Applied on Signal Patterns

To obtain data for comparison, a straight path of a known length s_w was walked ten times in a straight corridor. The data was collected with a 3D-accelerometer that was attached to the belt of the test walker and placed on the back. As the step length is a function of the walking speed, the walker tried to adjust the walking speed to normal, slower than normal, slow, faster than normal, and fast to obtain step samples with different step lengths. The test path was walked two times with each target speed. The steps were detected from the acceleration norms and signal patterns p_j, defined in (7)–(12), were computed from the data. From the signal patterns, square root, cube root, and 4th root were computed for each step. The step length model

$$\Delta s_k = K_{j,q}\, p_j(k)^q \tag{13}$$

was fitted to the data by estimating the scaling factor $K_{j,q}$ that relates Δs_k, the distance traveled during the kth step, with $p_j(k)^q$, where q is the exponent that defines the function to be applied on the signal pattern p_j computed for the kth step. In this example, values 1, $1/2$, $1/3$, and $1/4$ for q were tested; these correspond to the raw signal patterns and their square roots, cube roots, and 4th roots.

The scaling factors were estimated by taking the known total length of the distance walked during all the ten test walks and dividing it by the sum of the functions of the signal patterns computed for each detected step in all the test walks:

$$K_{j,q} = \frac{n_w s_w}{\sum_{i=1}^{n_w} \left(\sum_{k_i=1}^{n_i} p_j(k_i)^q \right)} \tag{14}$$

where n_w is the total number of test walks, n_i is the number of steps observed in the data set from the ith test walk, and $p_j(k_i)^q$ is the function of the signal pattern p_j during the k_ith step detected in the ith data set.

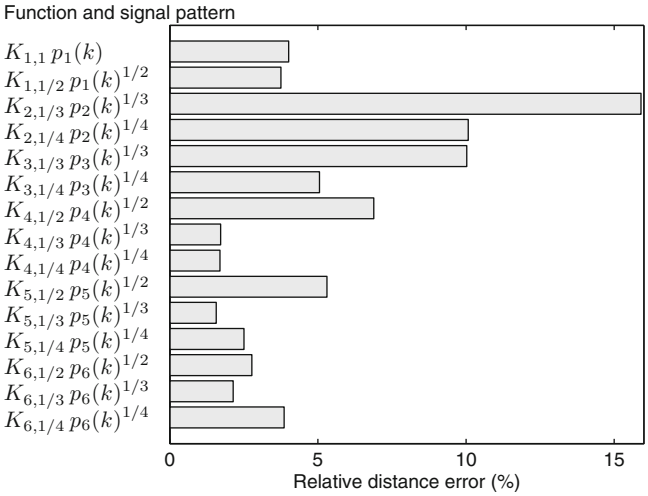

Fig. 5 Relative error in estimated distance traveled using step length estimates based on different functions of acceleration signal patterns

To compare the step length models with different signal patterns p_j and exponents q, the distances traveled on each test walk i were estimated using the obtained scaling factors:

$$\hat{s}_w(i,j,q) = K_{j,q} \sum_{k_i=1}^{n_i} p_j(k_i)^q. \tag{15}$$

From these estimates, the accumulated relative distance errors based on all the test walks were computed using

$$\varepsilon(j,q) = \frac{\sum_{i=1}^{n_w} |\hat{s}_w(i,j,q) - s_w|}{n_w \cdot s_w}. \tag{16}$$

The comparison of different functions applied on different signal patterns is illustrated in Fig. 5, where the 15 best estimation results in the terms of relative distance errors are shown.

3.3 PDR Mechanization

In the navigation technique called *dead reckoning* (DR) the position is estimated relative to the starting point by keeping track of the direction and distance traveled on each section of the route [23]. The idea is illustrated in Fig. 6. The process of

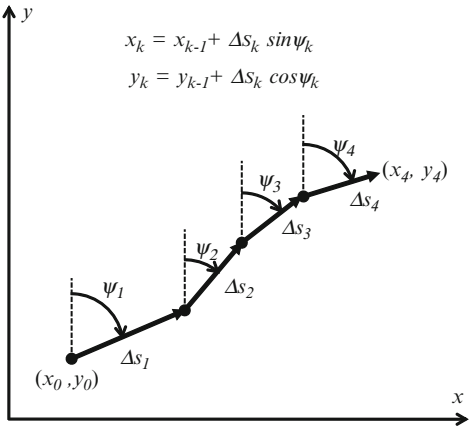

Fig. 6 Dead reckoning in two dimensions

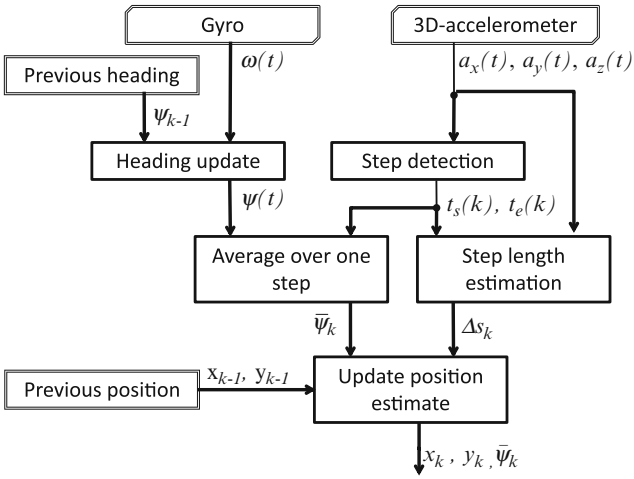

Fig. 7 Block diagram of the PDR algorithm

keeping track of position and direction of travel using inertial sensors is called mechanization. In PDR mechanization, the process involves also step detection and step length estimation, as shown in the diagram of Fig. 7. The PDR position estimate is computed by starting from initial coordinates, x_0, y_0, and initial heading angle ψ_0. As the DR method is not able to determine absolute positions, these initial estimates have to determined using alternative positioning methods, such as radio navigation or satellite based positioning.

While the position in PDR algorithm is updated only when step ends are detected, the heading is updated every Δt_g seconds, i.e., at the sampling frequency of the gyro:

$$\psi_\lambda = \psi_{\lambda-1} + \omega_\lambda \Delta t_g, \tag{17}$$

where ω_λ is the angular rate measurement by the gyro at the sampling instance $\lambda \Delta t_g$. In position estimation, a heading estimate representative of the whole step duration is needed. Therefore the heading is averaged over the step duration:

$$\bar{\psi}_k = \frac{1}{n_k} \sum_{\lambda \in \Lambda_k} \psi_\lambda, \qquad \Lambda_k = \left\{ \lambda : \lambda \text{ is an integer}, \frac{t_s(k)}{\Delta t_g} \leq \lambda < \frac{t_e(k)}{\Delta t_g} \right\} \tag{18}$$

where n_k is the number of samples in Λ_k. The heading and horizontal coordinates are propagated by

$$\begin{aligned} x_k &= x_{k-1} + \Delta s_k \cos \bar{\psi}_k \\ y_k &= y_{k-1} + \Delta s_k \sin \bar{\psi}_k \end{aligned} \tag{19}$$

where Δs_k is the estimated step length, i.e., the distance traveled during the step with index k. Position estimates that are based on step detection and step length estimation are available at step intervals Δt_k, which vary according to the walking style and the speed of the pedestrian.

Effect of Sensor Quality Grade to the Accuracy of PDR

Although PDR mechanization is not as sensitive to sensor errors as the traditional INS mechanization, the grade of sensors still has an effect to the performance of the PDR. In this section, the accumulation of errors in PDR is studied based on simple test cases.

From (7) to (12) it can be seen that the step length estimate is not sensitive to accelerometer bias: in p_2, p_3, p_5, and p_6 the bias is totally canceled out and in p_1 and p_4 its effect is small. Contrary to the bias error, the effect of the scale factor error on all other signal patterns except p_1 is directly proportional to the sensor error. However, taking square root, cube root or the fourth root of the signal pattern decreases the effect of accelerometer scale factor error on the step length estimate, as can be seen in Table 2.

If the scale factor error of the accelerometer is constant, its effect will be taken into account in the scaling factor of the step length model (14). In practice the scale factor error of a consumer grade accelerometer based on MEMS technology is slowly changing as a function of internal conditions of the sensing element, such as the temperature. If the temperature effect on the sensor scale factor at its maximum is 1%, then the effect on the estimated distance traveled is the same as the relative error of the evaluated function (Table 2) at the most. These values are small when compared with step length modeling errors, shown in Fig. 5 or reported in literature [11].

The effect of the gyro quality to PDR estimates can be analyzed by the simulation of a PDR system defined by (17)–(19). The effect of the gyro bias is simulated by using a scenario where the pedestrian walks with constant step length of 0.75 m and constant frequency of 2 steps/s along the positive x-axis. The gyro bias is assumed to be 25°/h, which is a typical bias instability of consumer grade gyros (Table 1). The development of heading error, error in estimated position and the position error

Table 2 Effect of 1% scale factor error in accelerometer to functions of signal patterns for step length estimation

Function	Raw $p_j(k)$	Square root $p_j(k)^{1/2}$	Cube root $p_j(k)^{1/3}$	Fourth root $p_j(k)^{1/4}$
Step length error (%)	1.00	0.50	0.33	0.25

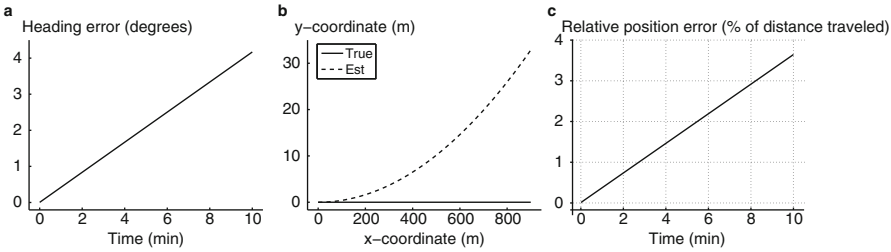

Fig. 8 Effect of 25°/h gyro bias when the pedestrian is walking with constant speed along the positive x-axis: (**a**) heading error, (**b**) true and estimated coordinates, and (**c**) relative position error

Table 3 Comparison of gyro grade with respect to the effect of uncompensated bias to the PDR error build-up

	Navigation	Tactical	Consumer
Bias instability (°/h)	0.0035	1	25
Time to 2% relative position error	27 days	2.3 h	5.5 min
Time to 3% relative position error	41 days	3.4 h	8.3 min
Time to 3° heading error	35 days	3.0 h	7.2 min

relative to the distance traveled is shown in Fig. 8. The heading error grows linearly (Fig. 8a), the error in the y-coordinate grows quadratically[4] with respect to the x-coordinate and time (Fig. 8b), and the relative position error with respect to the distance traveled grows almost linearly (Fig. 8c). With the best step length models, the long term average in the relative positioning error is about 2–3%, as can be seen in Fig. 5. With the given simulation parameters, the relative positioning error introduced by the gyro bias is smaller in the beginning, but exceeds 2% in less than 6 min and 3% in less than 9 min.

To compare the gyro grades described in Table 1, the simulations were also run with gyro instabilities typical to navigation and tactical grade gyros. The results are shown in Table 3.

The effect of the gyro scale factor error is simulated by using a scenario where the pedestrian first makes a 180° turn and then walks with a constant step length of 0.75 m and a constant frequency of 2 steps/s along the positive x-axis. The gyro scale

[4]The growth is almost quadratic with small heading errors; however, with larger heading errors, the sine and cosine functions in (19) bound the error growth.

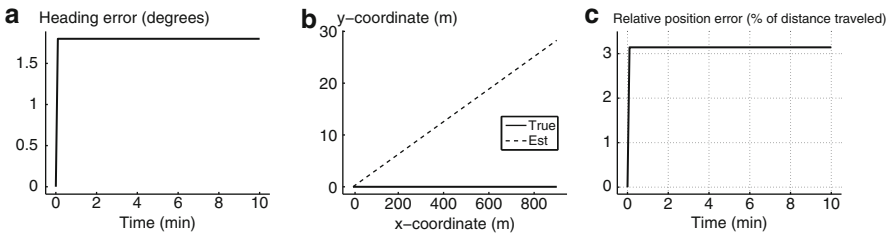

Fig. 9 Effect of 1% gyro scale factor error when the pedestrian has made a 180° turn from −180° and then walks with constant speed along positive *x*-axis: (**a**) heading error, (**b**) true and estimated coordinates, and (**c**) relative position error

Table 4 Comparison of gyro grade with respect to the effect of uncompensated scale factor error to the PDR error build-up

	Navigation	Tactical	Consumer
Scale factor error (%)	0.001	0.015	1
Constant heading error (degrees)	0.0018	0.027	1.8
Constant relative position error (%)	0.00314	0.047	3.14

factor error is assumed to be 1%, which is an upper bound of the gyro sensitivity over temperature of a consumer grade gyro [31]. The heading error, the error in the estimated position, and the position error relative to the distance traveled are shown in Fig. 9. In this simulation, the heading error grows in the turn to 1.8° and then stays constant, as the scale factor error has an effect only when the gyro senses a non-zero angular rate (Fig. 9a). Due to the constant heading error, the position error grows linearly with respect of time and *x*-coordinate (Fig. 9b). In the initial turn, the position error relative to the distance traveled jumps directly to more than 3% (Fig. 9c). That is, with the parameters used in this simulation and after a 180° turn, the error due to the gyro scale factor error is larger than the error introduced by the best step length models in Fig. 5.

To compare the gyro grades described in Table 1, the simulations were also run with gyro scale factor errors typical to navigation and tactical grade gyros. The results are shown in Table 4.

It should be noted that the simulation results given in this section apply only on PDR mechanization of inertial sensors. The growth of position error is much faster with traditional INS mechanization, partly due to the low speed of the pedestrian and partly due to the algorithm simplifications allowed by the characteristics of pedestrian movements. Another important remark considers the effect of the tilt error of the heading gyro: the simulations assume that the sensitive axis of the gyro is aligned with vertical. However, in practice the sensor unit easily gets tilted by a couple of degrees, which introduces a scaling error to the gyro output.

4 Human Motion Classification with Accelerometers

In addition to providing data for navigation purposes, inertial sensors can be used for motion classification. As shown in Fig. 10, the waveform of the norm of acceleration (6) has different characteristics depending on motion mode of the person carrying the unit. When walking, foot impacts clearly increase the variability of the signal. When driving a car, engine vibrations, vehicle accelerations, and road imperfections cause variations which are smaller than those occurring during walking, yet distinguishable from the case of a stationary device where the only source of variation is measurement noise.

In order to have a means for identifying these motion modes, features such as sample variance or peak frequency need to be extracted from the acceleration data. Figure 11 shows two such features: the sample standard deviation σ and the peak frequency from non-overlapping five-second windows. In this example, the classification is relatively easy, as the characteristics are clearly distinguishable. In practice, there are more motion modes to classify and proper statistical tools are needed to obtain useful classification results. In this section a brief introduction to such tools is given.

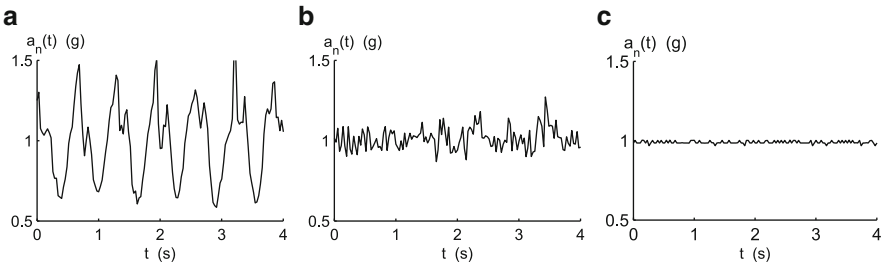

Fig. 10 Norm of accelerometer output in different motion modes: (**a**) walking, $\sigma = 0.24$ g, (**b**) driving, $\sigma = 0.071$ g, and (**c**) stationary, $\sigma = 0.0084$ g

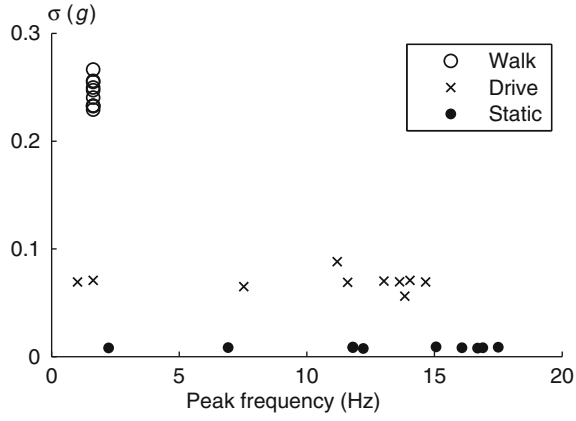

Fig. 11 Standard deviation and peak frequency as features

4.1 Pattern Recognition

In one of the simplest cases, pattern recognition is discrimination between r multivariate normal populations. The Bayes theorem is applied to obtain the probability of the originating population class (motion mode) given the statistics obtained from the accelerometer data. The underlying assumption of Gaussian distribution of the features is obviously invalid for features such as sample variance, but it makes the classification very straightforward. A training data set with labeled motion modes is needed to obtain the class means μ_j and covariances Σ_j for each class j. Then, according to the model, the future observations collated to a q-dimensional feature vector $\mathbf{z}$ are distributed as

$$\mathbf{z}_j \sim N(\mu_j, \Sigma_j). \tag{20}$$

It should be stressed that the training data set is, in practice, often very small, and thus the mean vector $\mu_j \in \mathbb{R}^q$ and the covariance matrix $\Sigma_j \in \mathbb{R}^{q\times q}$ are actually estimates of the true model parameters. Further simplification is made by assuming that the training data cannot be used to specify the prior probability $P(C = j)$, the probability of event that the future observation comes from class j. Under these assumptions, Bayes' theorem can be applied to obtain

$$P(C = j|\mathbf{z}) = \frac{p_{\mathbf{z}_j} P(C = j)}{p_{\mathbf{z}}} \tag{21}$$

where

$$p_{\mathbf{z}} = \sum_{i=1}^{r} p_{\mathbf{z}_i} P(C = i). \tag{22}$$

The actual classification result is obtained by finding the class that maximizes the posterior probability $P(C = j|\mathbf{z})$.

4.2 Feature Selection

Two very important features for classification of motion modes were already mentioned, i.e., variance and peak frequency. When selecting more features it is important to keep the actual application in mind—if the selected features are not useful in distinguishing between the motion modes, they should not be included in the classifier due to numerical problems that may arise. Some useful features are [6]:

- Sample variance
- Peak frequency
- Amplitude of the peak frequency
- Slope of the peak
- Change in the peak frequency over 4 sub-frames

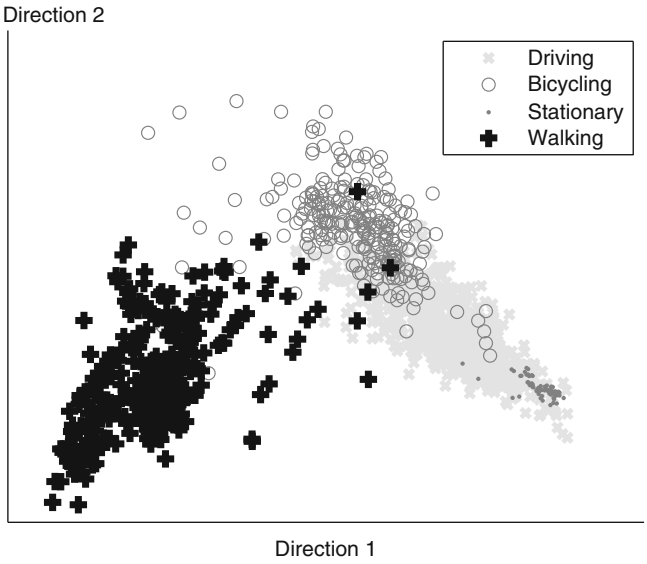

Fig. 12 Features projected onto the two best linear discriminant directions

- Energy of the signal, in four frequency bands
- Energy of the signal near to the peak frequency
- Maximum value minus minimum element

To make the feature selection easier, there exist efficient algorithms that can be used to remove or compress irrelevant and redundant features via linear transformations [32]. An example of the two most relevant features after such a transformation is shown in Fig. 12. This figure shows features collected from several persons, and it can be seen that there is significant overlap between the modes. In particular, the "driving" mode spreads over the "stationary" and "bicycling" modes. This overlap implies that the selected features cannot distinguish the modes exactly, and classification errors are thus anticipated.

4.3 Classification Accuracy

In practice it is impossible to implement a classifier that makes no mistakes; misclassifications will occur from time to time. From the viewpoint of the application designer, the classification accuracy must be evaluated for two different cases: (a) the expected misclassification rate prior to observing the features, and (b) the probability of misclassification given the observed feature vector. For the former, the overlap in the training data is a good indicator. For the latter, (21) directly gives such probability, but this value is often too optimistic. This is due to the underlying

assumptions: prior probabilities are known, the list of classes is exhaustive, feature data follow Gaussian distribution, and the distribution parameters from the training data contain no sampling errors.

For obtaining a realistic values for misclassification rates, cross-validation tests or completely new labeled training is required. If the training can be done individually and the number of classes can be limited to five, a misclassification rate better than 10% can be expected [12]. On the other hand, if the number of classes is increased to nine, misclassification rates worse than 50% can be expected for the most difficult motion modes [16]. To tolerate misclassifications, the application should not apply the classification result at all if the result seems too uncertain. For this purpose, a partial classification algorithm should be implemented. In partial classification the option of not classifying a situation at all is reserved [4].

4.4 Areas of Application

Accurate motion mode classification would enable several applications. For example, motion mode information would be valuable for remote monitoring of elderly people. For navigation applications the detection of Walking-mode allows using PDR, and the detection of Static-mode can be used to save power by turning off the GPS receiver [28]. In principle, motion mode classification methods can be used in any area where human motion is involved and the subjects exhibit distinct signatures [2]. The list of available applications is expected to grow as most of the modern smartphones are equipped with MEMS IMUs.

5 Summary

With the development of low-cost MEMS accelerometers and gyroscopes, more and more applications become achievable. Many applications can be easily implemented on portable media devices (smartphones, etc). Since inertial sensors measure motion parameters, the solution is based on physical properties specific to the application; emerging applications are usually significantly different from the original use of inertial sensors, i.e., navigation. One way to improve the performance is to calibrate the inertial sensors and to filter the sensor data appropriately. Understanding of physical principles of the application helps to use effectively the inertial sensors. In this chapter, an introduction to inertial sensor applications was provided. Such a concise presentation did not permit in-depth treatment of individual topics. More information about the additional topics can be found, e.g., in [2, 24, 29] and the references cited therein.

References

1. Allan, D.W.: Statistics of atomic frequency standards. Proc. IEEE **54**(2), 221–230 (1966)
2. Altun, K., Barshan, B., Tunçel, O.: Comparative study on classifying human activities with miniature inertial and magnetic sensors. Pattern Recogn. **43**, 3605–3620 (2010)
3. Armenise, M.N., Ciminelli, C., Dell'Olio, F., Passaro, V.: Advances in Gyroscope Technologies. Springer Verlag (2010)
4. Broffit, J.D.: Nonparametric classification. In: P.R. Krishnaiah, L.N. Kanal (eds.) Handbook of Statistics 2. North-Holland (1990)
5. Brown, R.G., Hwang, P.Y.C.: Introduction to Random Signals and Applied Kalman Filtering, 3rd edn. John Wiley & Sons (1997)
6. Collin, J.: Investigations of self-contained sensors for personal navigation. Dr. Tech. thesis, Tampere University of Technology (2006). URL http://webhotel.tut.fi/library/tutdiss/pdf/collin.pdf
7. Foxlin, E.: Pedestrian tracking with shoe-mounted inertial sensors. IEEE Computer Graphics and Applications **25**(6), 38–46 (2005)
8. Gianchandani, Y.B., Tabata, O., Zappe, H.P.: Comprehensive microsystems. Elsevier (2008)
9. IEEE Std 528-2001: IEEE standard for inertial sensor terminology. standard, The Institute of Electrical and Electronics Engineers, Inc., New York, NY, U.S.A. (2001)
10. IEEE Std 647-1995: IEEE standard specification format guide and test procedure for single-axis laser gyros. standard, The Institute of Electrical and Electronics Engineers, Inc., New York, NY, U.S.A. (1996)
11. Jahn, J., Batzer, U., Seitz, J., Patino-Studencka, L., Gutiérrez Boronat, J.: Comparison and evaluation of acceleration based step length estimators for handheld devices. In: Proc. Int. Conf. on Indoor Positioning and Indoor Navigation, pp. 1–6. Zurich, Switzerland (2010)
12. Kantola, J., Perttunen, M., Leppänen, T., Collin, J., Riekki, J.: Context awareness for GPS-enabled phones. In: Proc. ION ITM, pp. 117–124. San Diego, CA (2010)
13. Käppi, J., Syrjärinne, J., Saarinen, J.: MEMS-IMU based pedestrian navigator for handheld devices. In: Proc. ION GPS, pp. 1369–1373. Salt Lake City, UT (2001)
14. Keshner, M.S.: $1/f$ noise. Proc. IEEE **70**(3), 212–218 (1982)
15. Kirkko-Jaakkola, M., Collin, J., Takala, J.: Bias prediction for MEMS gyroscopes. IEEE Sensors J. (2012). DOI 10.1109/JSEN.2012.2185692
16. Könönen, V., Mäntyjärvi, J., Similä, H., Pärkkä, J., Ermes, M.: Automatic feature selection for context recognition in mobile devices. Pervasive Mob. Comput. **6**, 181–197 (2010)
17. Krobka, N.I.: Differential methods of identifying gyro noise structure. Gyroscopy and Navigation **2**, 126–137 (2011)
18. Ladetto, Q.: On foot navigation: continuous step calibration using both complementary recursive prediction and adaptive Kalman filtering. In: Proc. ION GPS, pp. 1735–1740. Salt Lake City, UT (2000)
19. Leland, R.P.: Mechanical-thermal noise in MEMS gyroscopes. IEEE Sensors J. **5**(3), 493–500 (2005)
20. Levi, R.W., Judd, T.: Dead reckoning navigational system using accelerometer to measure foot impacts. U.S. Patent 5,583,776 (1996)
21. Meriheinä, U.: Method and device for measuring the progress of a moving person. U.S. Patent 7,962,309 (2007)
22. Mezentsev, O., Collin, J., Lachapelle, G.: Pedestrian Dead Reckoning – A Solution to Navigation in GPS Signal Degraded Areas. Geomatica **59**(2), 175–182 (2005)
23. Misra, P., Enge, P.: Global Positioning System: Signals, Measurements, and Performance, 2nd edn. Ganga–Jamuna Press (2006)
24. Roetenberg, D., Luinge, H., Slycke, P.: Xsens MVN: Full 6DOF human motion tracking using miniature inertial sensors. Tech. rep., Xsens Motion Technologies BV (2009)
25. Savage, P.G.: Laser gyros in strapdown inertial navigation systems. In: Proc. IEEE Position, Location, and Navigation Symp. San Diego, CA (1976)

26. Sierociuk, D., Tejado, I., Vinagre, B.M.: Improved fractional Kalman filter and its application to estimation over lossy networks. Signal Process. **91**(3), 542–552 (2011)
27. Stirling, R., Collin, J., Fyfe, K., Lachapelle, G.: An innovative shoe-mounted pedestrian navigation system. In: Proc. ENC GNSS, pp. 110–115. Graz, Austria (2003)
28. Syrjärinne, J., Käppi, J.: Method and apparatus for lowering power use by a ranging receiver. U.S. Patent 7,409,188 (2008)
29. Titterton, D.H., Weston, J.L.: Strapdown Inertial Navigation Technology, 2nd edn. American Institute of Aeronautics and Astronautics, Reston, VA (2004)
30. Voss, R.F.: $1/f$ (flicker) noise: A brief review. In: Proc. 33rd Ann. Symp. Frequency Control, pp. 40–46 (1979)
31. VTI Technologies Oy: SCC1300-D04 combined gyroscope and 3-axis accelerometer with digital SPI interfaces. rev. 1.0.3. Doc.Nr. 82 1131 00 A, Data sheet (2010)
32. Webb, A.: Statistical Pattern Recognition, 2nd edn. John Wiley & Sons, LTD (2002)
33. Xsens MVN – inertial motion capture. URL http://www.xsens.com/en/general/mvn